



# Enhanced photocatalytic performance of graphene–ZnO nanoplatelet composite thin films prepared by electrostatic spray deposition

Bhavana N. Joshi<sup>1</sup>, Hyun Yoon<sup>1</sup>, Seung-Heon Na, Jae-Young Choi, Sam S. Yoon\*

*School of Mechanical Engineering, Korea University Anamdong, Seongbukgu, Seoul 136-713, Korea*

Received 21 August 2013; received in revised form 13 September 2013; accepted 14 September 2013

Available online 20 September 2013

## Abstract

Graphene–ZnO (G–ZnO) composite thin films were produced using the electrostatic spray deposition technique (ESD). The effects of the concentration of graphene and annealing temperature on the structural and photocatalytic properties of the G–ZnO films were studied by X-ray diffraction, scanning electron microscopy, atomic force microscopy, Raman spectroscopy, and UV–visible spectroscopy. We demonstrated that the G–ZnO films exhibit enhanced activities towards the photodegradation of methylene blue dye. A G–ZnO film with 0.1 wt% graphene that was annealed at 300 °C showed the highest photo-degradation activity. We found that the incorporation of graphene reduced electron–hole recombination in the ZnO film.

© 2013 Elsevier Ltd and Techna Group S.r.l. All rights reserved.

*Keywords:* D. ZnO; Graphene-ZnO; Photocatalyst; Methylene Blue

## 1. Introduction

Photocatalytic degradation of toxic dyes by semiconductor photocatalysts, such as titanium dioxide (TiO<sub>2</sub>) and zinc oxide (ZnO), has been extensively studied and utilized because of its effectiveness and sophistication, as well as the non-toxicity of its byproducts. Among the various semiconductor materials, ZnO (which has a bandgap of 3.37 eV) is abundant, relatively inexpensive, biocompatible, strongly oxidative, better than TiO<sub>2</sub> for the degradation of certain organic dyes, and can be manufactured under ambient conditions [1]. Recent publications have shown that ZnO can be used for the degradation of toxic dyes, as well as sterilization of bacteria [2,3]. However, its photocatalytic performance depends on the surface area of the photocatalyst and the rate of recombination of the photo-induced electrons with their corresponding holes [4]. Few studies have investigated the fabrication of photocatalytic composite materials, such as carbon nanotubes or graphene-doped ZnO (heterogeneous photocatalysis), to evaluate the possibility of reducing the recombination rate of charge carriers [5–7] and enhance the

potential for mineralizing toxic organic pollutant dyes [6]. Graphene, which comprises two-dimensional sheets of carbon atoms arranged in a hexagonal lattice structure, has excellent electrical conductivity and mechanical properties. Thus, graphene-doped ZnO (G–ZnO) is expected to have improved electron transport during photocatalysis through reduction of the charge recombination rate, which should enhance the photocatalytic performance. Additionally, the inclusion of graphene will increase the surface area and roughness of the composite film, which will enhance the photoelectrochemical reaction between the surface of the catalyst and organic pollutants. Therefore, the morphology of the G–ZnO composite film also plays an important role in the photocatalytic process.

Numerous methods have been employed for the deposition of ZnO films, including RF magnetron sputtering [8], electron beam evaporation [9], metal organic chemical vapor deposition [10], and pulsed laser deposition [11]. ZnO films can also be fabricated through non-vacuum techniques, such as sol–gel [12], spray pyrolysis [13], and electrostatic spray deposition (ESD) [14]. Graphene films have also been deposited through chemical vapor deposition (CVD) [15], spin coating [16], ESD [17], and spraying [18]. Among these deposition processes, ESD is the most attractive because it produces extremely fine (nanosized), self-dispersive (non-aggregating), highly wettable

\*Corresponding author.

E-mail address: [skyoona@korea.ac.kr](mailto:skyoona@korea.ac.kr) (S.S. Yoon).

<sup>1</sup>Equal contribution.

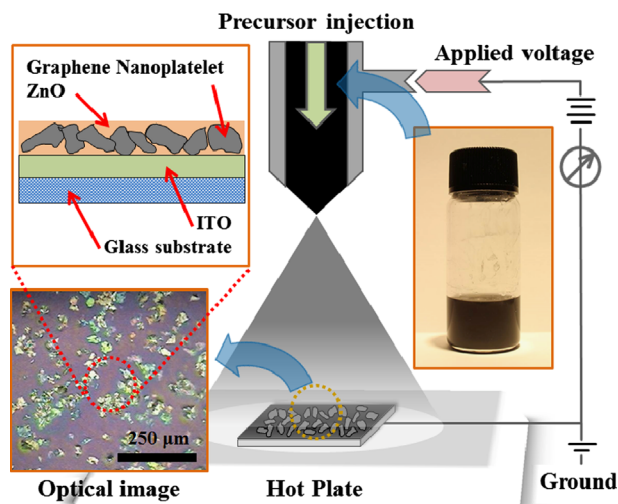


Fig. 1. Experimental schematic used for deposition of G-ZnO thin films.

(electrowetting), and adhesive droplets that yield a uniform coating on the substrate in addition to being the most cost-effective method. The schematic of the ESD setup is illustrated in Fig. 1, and additional details are provided in our previous publications [19,20].

Lam et al. [21] reviewed and summarized recent research on ZnO photocatalytic systems for the degradation of organic dyes. Photocatalysis using modified films with varying morphologies, such as nanoplatelets, nanorods, nanosheets, nanoflowers, nanocups, and nanoneedles, was discussed. These nanostructures possess different surface-to-volume ratios. As this ratio increases, the rate of electron–hole transfer from the semiconducting material to the absorbing molecules also increases, thereby enhancing photocatalytic performance. Liu et al. [22] synthesized ZnO nanocrystals on graphene nanosheets as a powder using a microwave-assisted approach. They studied the decolorization of rhodamine-B and methylene blue (MB) by irradiating the sample with visible light in the presence of the G–ZnO powder: 6.9 mM Zn mixed with graphene yielded the best synergism for degradation of the dyes. A G–ZnO hybridized powder photocatalyst was also reported by Xu et al. [6], who revealed that ZnO loaded with 2 wt% graphene degraded MB four times more effectively than pure ZnO after irradiation with UV light at a wavelength of 254 nm. Li et al. [5] synthesized a G–ZnO composite powder using the chemical deposition method for the photocatalytic degradation of rhodamine-B under UV and visible light. Thus, G–ZnO photocatalysts have already been proven in a mobilized mode (i.e., in the powder form in aqueous media within a fluidized reactor for photocatalytic studies). However, the mobilized mode ultimately requires separation of the fine powder from the aqueous media. This separation is often difficult because the fine powder remains in a colloidal state and does not settle sufficiently, which results in the need for additional equipment. To circumvent this technological difficulty, an immobilized mode in the form of a G–ZnO film fabricated by ESD, is proposed herein for the first time. In our

previous work, we reported the deposition of ZnO thin films (without graphene) by ESD for transparent conducting oxide applications [20]. Since vacuum conditions are not required, the ability to produce nanoscale-thickness films in a cost-effective manner with high deposition efficiency makes it practical to use ESD for the fabrication of G–ZnO composite photocatalytic immobilized films. The effects of graphene concentration (weight percentage) and annealing temperature on the surface morphology and photocatalytic response of the film will be discussed in this report. We will also demonstrate that the graphene concentration has a significant effect on film growth and photocatalytic degradation of MB dye.

## 2. Experimental

### 2.1. Precursor

The precursor solution for ESD coating comprised zinc acetate dihydrate (ZnAc;  $\sim 0.1$  M) dissolved in propylene glycol (PG). Graphene flakes were dispersed in alcohol (BMSTECH, Korea), and the dispersion was then mixed into the ZnAc–PG solution. The concentration of the graphene solution varied from 0.1 to 1 and up to 5.0 wt%. Concentrations higher than 5.0 wt% resulted in poor adhesion of the film. A few drops of water were added to the graphene–ZnAc solution for proper dilution and dispersion of the graphene, and the solution was then stirred for 30 min. A pre-cleaned sample of soda-lime glass coated with indium tin oxide (ITO) was used as the base substrate. The ITO layer prevents the migration of Na and other foreign atoms from the glass, which might reduce the photocatalytic activity of the deposited G–ZnO film.

The precursor solution was administered from a syringe pump at a flow rate adjusted to the yield of a stable Taylor cone, which produces the smallest droplets possible under the given operating conditions (see Fig. 1). The inner diameter of the nozzle was 4 mm. A voltage-supply wire was attached to the charging needle (i.e., anode), and the substrate was grounded (to act as the cathode). The precursor flow rate was set at 120  $\mu\text{L}/\text{h}$  with applied voltages of 12–14 kV. Typically, it took approximately 20–30 min to yield a 150–175 nm thick G–ZnO film. The cone angle of the atomizing spray from the Taylor cone was approximately  $40^\circ$ , which provides circular coverage with a 3 cm diameter at a 4 cm nozzle-to-substrate distance. While spraying the G–ZnO precursor, the temperature of the stationary substrate was initially maintained at  $90^\circ\text{C}$  to ensure pyrolysis and subsequent formation of a solid thin film. Finally, the films were annealed in a closed furnace at  $300$ – $500^\circ\text{C}$  in a two-step process involving 10 min at  $200^\circ\text{C}$  to remove any remaining PG and 30 min at the elevated temperatures mentioned above to crystallize the ZnO.

### 2.2. Film characterizations

The crystalline structures of the pure ZnO and G–ZnO thin films were identified by X-ray diffraction (XRD, Rigaku, D/max-2005)

with Cu K $\alpha$  radiation ( $\lambda=0.154$  nm). The surface morphologies and cross-sectional views of the films were imaged using a high-resolution scanning electron microscope (HR-SEM, Philips, L30SFEG at 10 kV). A non-contact-mode atomic force microscope (AFM; Park Systems, XE-100) was used to examine the surface morphology and roughness of the electrospayed G–ZnO film. A Raman spectrometer was used to observe the graphene content and defects of the film. The optical absorption properties of the G–ZnO films within the spectral region of 300–800 nm were evaluated using a UV–vis spectrometer (Mecasys Co., Ltd., Optizen POP).

### 2.3. Photocatalysis

The photocatalytic performances of all G–ZnO films were obtained under weak UV exposure ( $0.6$  mW/cm $^2$ ). A solution of MB is often used as the model pollutant, since it decomposes through both direct oxidation and via the OH radicals generated during the photocatalytic process [23,24]. The MB solution (#M2661, 0.1 wt% solution in water, Samchun Chemical, Korea) was mixed with deionized water at a 1:400 volume ratio. The G–ZnO film was placed inside a Pyrex vessel and sealed with a Pyrex petri dish. The concentration of MB inside the vessel decreased as photocatalysis proceeded, and the concentration was monitored using a UV–vis spectrometer. The absorbance data from the UV–vis spectra were obtained by converting the transmittance data using the Beer–Lambert law [25,26]. All tests were repeated at least three times to ensure the reliability and repeatability of the results.

### 3. Results and discussion

The crystal structures and orientations of the pure ZnO and G–ZnO thin films on the ITO substrates were examined by X-ray diffraction (XRD) in the range of  $20^\circ < 2\theta < 70^\circ$ . Fig. 2 shows the XRD patterns of the various samples of the films (i.e., with an ITO substrate, pure ZnO, and 0.1, 1.0, and 5.0 wt % G–ZnO films) annealed at 300, 400, and 500 °C. The diffraction peaks denoted by diamonds (◆) indicate that the ZnO films are polycrystalline with no preferential orientation. The peaks are consistent with the diffraction planes of the hexagonal wurtzite structure of ZnO, as confirmed by JCPDS data card no. 36-1451. The peaks observed at diffraction angles of  $31.4^\circ$ ,  $33.9^\circ$ , and  $36.1^\circ$  correspond to the (100), (002), and (101) planes of ZnO, respectively. The intensities of the ZnO peaks for the 5.0 wt% G–ZnO film are relatively weak. The diffraction peaks corresponding to the ITO substrate are identified by black circles (●) in Fig. 2. The graphene peaks at  $26.1^\circ$  (denoted by ▼) are also observed in the diffraction patterns of the 0.1, 1.0, and 5.0 wt% G–ZnO films annealed at 300 °C [27]. However, the intensities of the graphene peaks in the patterns of the 1.0 and 5.0 wt% G–ZnO films gradually decrease at higher annealing temperatures. Fig. 3 shows a comparison of the XRD peaks of graphene at various annealing temperatures: as the annealing temperature increases, the graphene peak diminishes and eventually disappears. This phenomenon was originally described by Wang et al. [28], who noted that graphene nanosheets

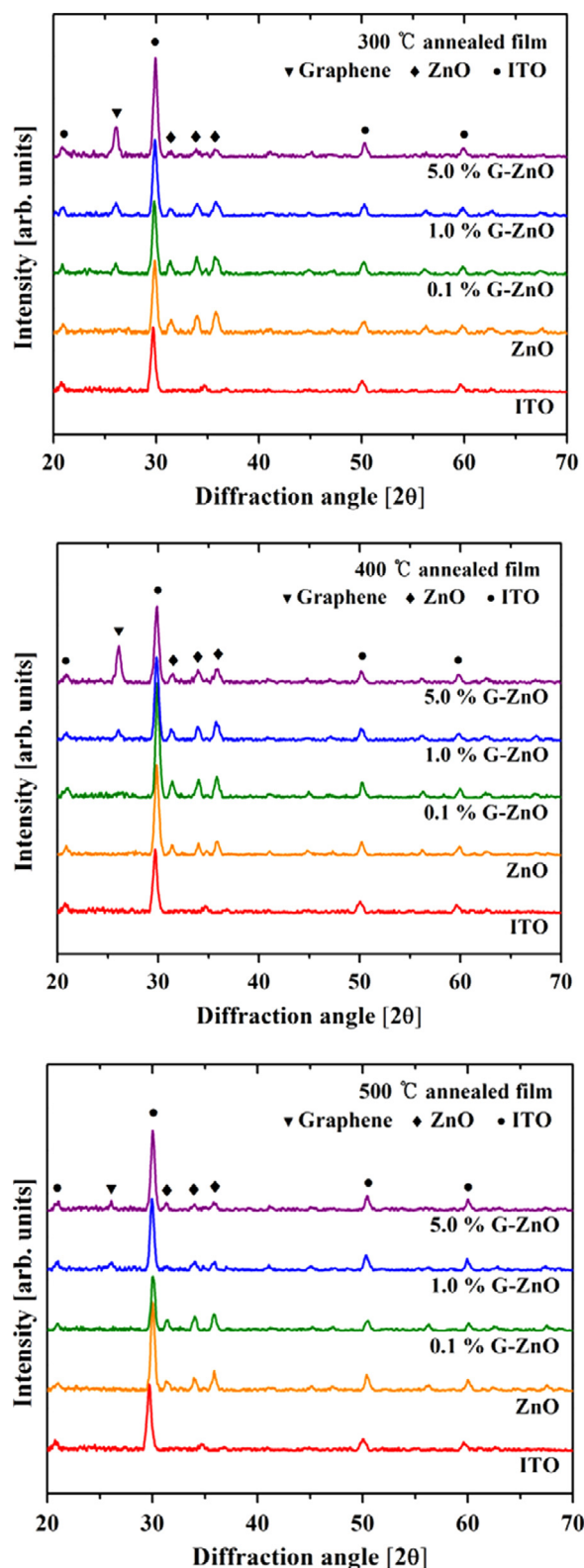


Fig. 2. XRD of G–ZnO thin films on ITO substrate annealed at (a) 300, (b) 400 and (c) 500 °C.

have a relatively low thermal stability. By thermogravimetric analysis, they revealed that graphene decomposed from the films during annealing in air at temperatures of 250–600 °C. Xi et al.

[29] also observed graphene decomposition from graphene nanosheets functionalized with bovine serum albumin above an annealing temperature of 450 °C. Thus, we suspect that the absence of the graphene peaks after annealing at 400 and 500 °C in our experiment is due to decomposition of graphene during annealing in air.

SEM surface views of the ZnO and G–ZnO films with different graphene concentrations annealed at 300 °C are shown in Fig. 4. The pure ZnO film shows small grains with few holes on the surface of film, and the surface views of the G–ZnO films clearly show the graphene sheets. The graphene sheet content clearly increases as the graphene concentration increases from 0.1 to 5.0 wt%.

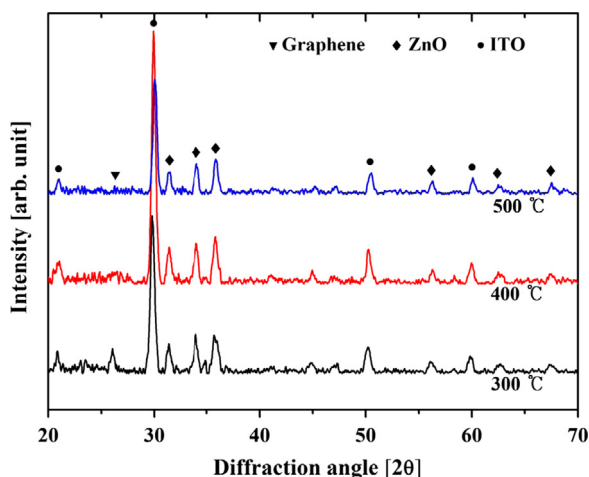


Fig. 3. XRD of 0.1 wt% G–ZnO thin films on ITO substrate annealed at different temperatures.

Fig. 5 shows 2D and 3D AFM images of the pure ZnO and G–ZnO films with a concentration of 0.1 wt%. Their measured surface roughness ( $R_a$ ) values are 5.38 and 34.48 nm, respectively. It is important to note that the surface roughness of the ITO substrate was 0.5 nm. The AFM images of the 0.1 wt% G–ZnO films show irregularly shaped graphene sheets that are spread out and a few micrometers in length. The graphene sheet yielded higher surface roughness.

As shown in Fig. 6, the Raman spectra of the G–ZnO films with various graphene concentrations annealed at 300 °C show a G band ( $\sim 1573 \text{ cm}^{-1}$ ) corresponding to the  $\text{sp}^2$  hybridized carbon and a D band ( $\sim 1360 \text{ cm}^{-1}$ ) originating from the disordered carbon. The 2D peak at  $\sim 2722 \text{ cm}^{-1}$ , which corresponds to the overtone of the D band, indicates the increased disorder of graphene. As expected, the spectra of ITO and ZnO did not contain any graphene peaks. The strong peaks due to the G and 2D bands of graphene are observed in the films annealed at 300 and 400 °C. However, there were no graphene peaks in the Raman spectra of the films annealed at 500 °C (not shown here), as previously indicated by the XRD analyses (Fig. 3).

The optical transmittances of the G–ZnO thin films were measured using a UV–vis spectrometer, as shown in Fig. 7. Contrary to our hypothesis, the ITO–ZnO film had a greater transmittance than the pure ITO film in the region of  $\lambda > 600 \text{ nm}$ . This occurs because annealing improves the ITO–ZnO film transmittance, whereas the pure ITO film was not annealed. Overall, the transmittance decreased as the graphene content increased. This drastic transmittance change when  $\lambda < 370 \text{ nm}$  represents the characteristic absorption edge of ZnO [30]. The absorption edge shifts towards higher wavelengths for the G–ZnO films, compared to that of the ITO–ZnO film, because the bandgap narrows [31].

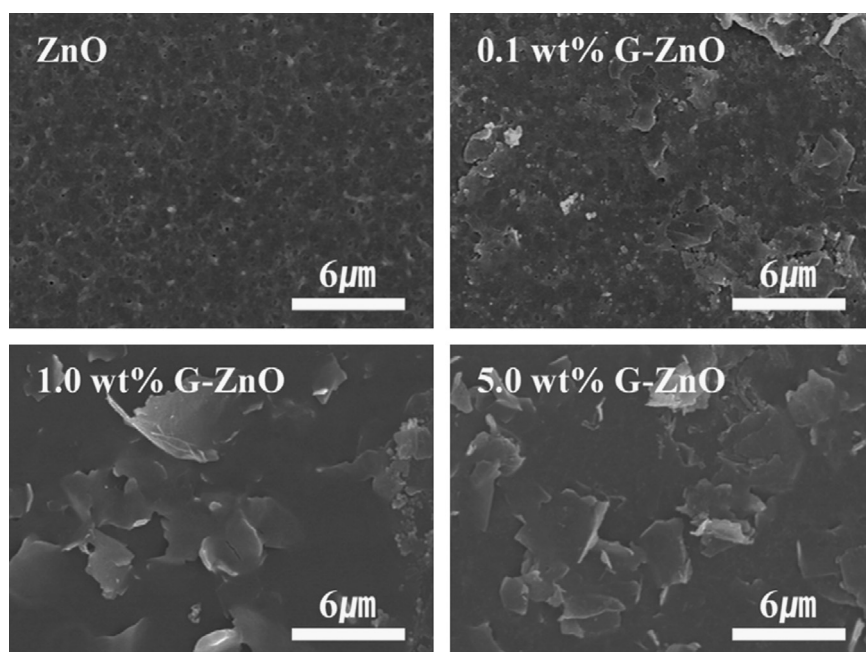


Fig. 4. SEM surface view of thin films with different graphene concentrations annealed at 300 °C.

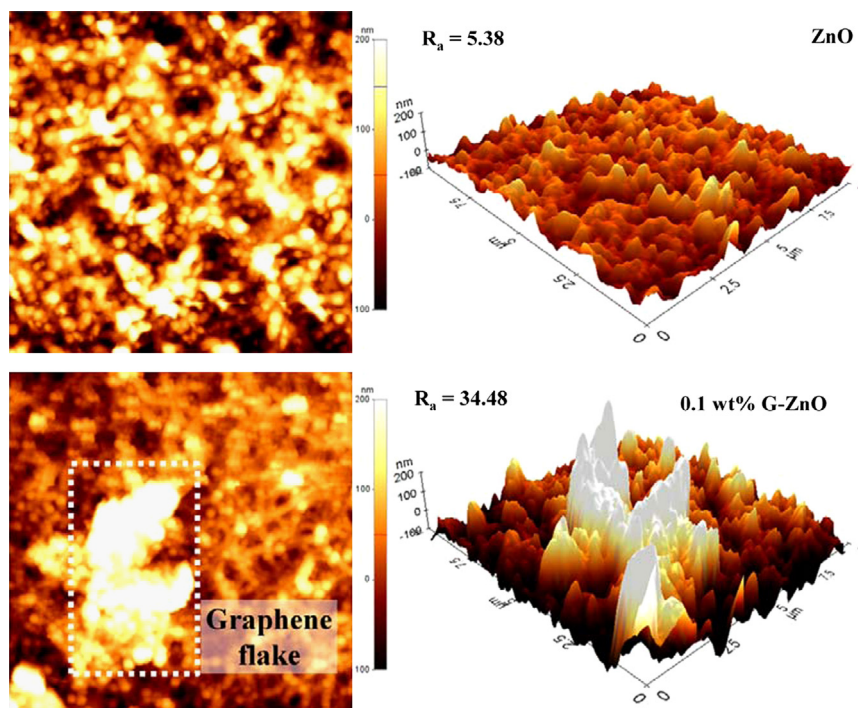
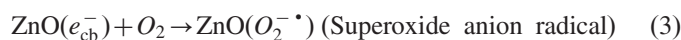
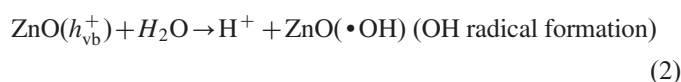
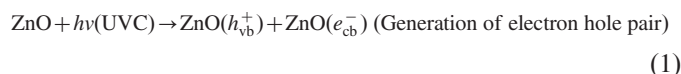


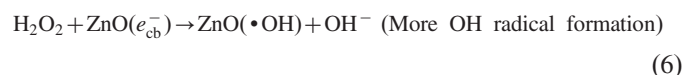
Fig. 5. 2D and 3D view AFM images of the ZnO and 0.1 wt% G-ZnO films annealed at 300 °C. Note, that  $R_a$  is the surface roughness.

The photocatalytic activities of the ZnO and G-ZnO films were evaluated via decolorization of the aqueous MB dye. Fig. 8 displays the effect of varying the graphene concentration in the G-ZnO films and the effect of the photocatalytic activity of the pure ZnO film on the degradation of the MB dye after 2 h of UV irradiation. Since the high annealing temperature (e.g., ~500 °C) resulted in degradation of the graphene, we used the films annealed at 300 °C to evaluate the effect of the graphene content on the degradation of the MB dye. As expected, Fig. 8 shows that the ZnO film alone, without graphene doping, also showed significant photodegradation activity. With respect to the effect of graphene doping, the G-ZnO film with 0.1 wt% graphene showed the greatest photodegradation since its absorbance was the smallest. A photodegradation study on the 0.5 wt% G-ZnO film was also carried out. However, the difference between the degradation of MB with 0.5 wt% and 1.0 wt% G-ZnO films was negligible; therefore, the 0.1 and 1.0 wt% G-ZnO thin films are compared in this paper. The reaction mechanism of the photocatalytic decolorization of the MB solution in the presence of ZnO can be explained by the following reaction steps [2,32]:



The photocatalytic activity of ZnO begins upon irradiation with UV light ( $\lambda=254$  nm), which generates electron-hole

pairs via elevation of a generated free electron to the conduction band leaving behind a hole ( $h_{\text{vb}}^+$ ) in the valence band. In the presence of oxygen, scavenging electrons yield superoxide radicals ( $\text{O}_2^- \cdot$ ) while the holes react with water from the surface to form hydroxyl radicals ( $\cdot\text{OH}$ ). Recombination of electrons with their holes is prevented by the transfer of electrons from ZnO to graphene, which generates additional superoxide and hydroxyl radicals.



These hydroxyl and superoxide radicals react with the MB dye (reaction steps (7) and (8)) to yield degradation products such as  $\text{CO}_2$ ,  $\text{NO}_3^-$ ,  $\text{NH}_4^+$ , and  $\text{SO}_4^{2-}$ .

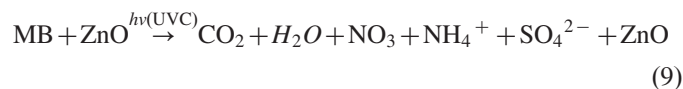


Fig. 9 displays the transitional MB decomposition, non-dimensionalized by the initial concentration (i.e.,  $C/C_0$ ) after 0–2 h of UV irradiation. It is noteworthy that direct exposure of MB to UV radiation without any catalytic materials did not result in any evident degradation, which indicates the relatively weak intensity of the UV radiation. However, the photocatalytic activities of the ZnO and G-ZnO films are clearly shown

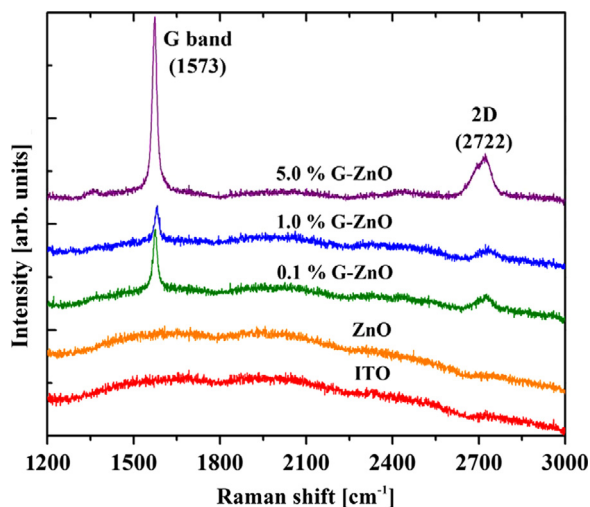


Fig. 6. Raman spectra of ITO, ZnO, and G–ZnO films of various concentrations annealed at 300 °C.

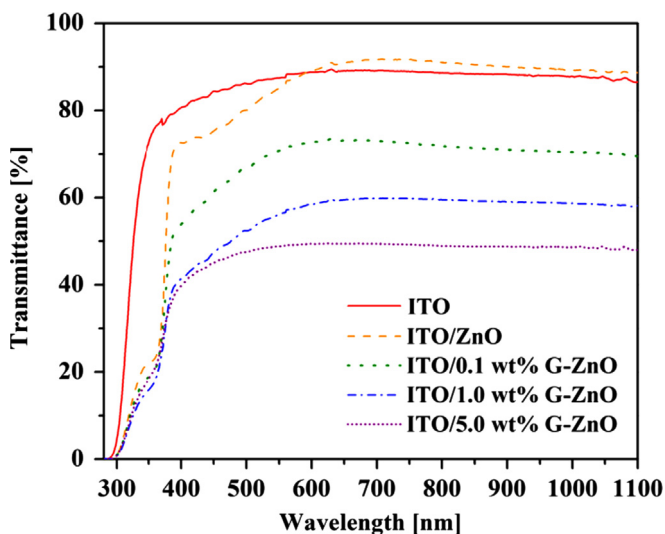


Fig. 7. UV transmittance spectra of films annealed at 300 °C.

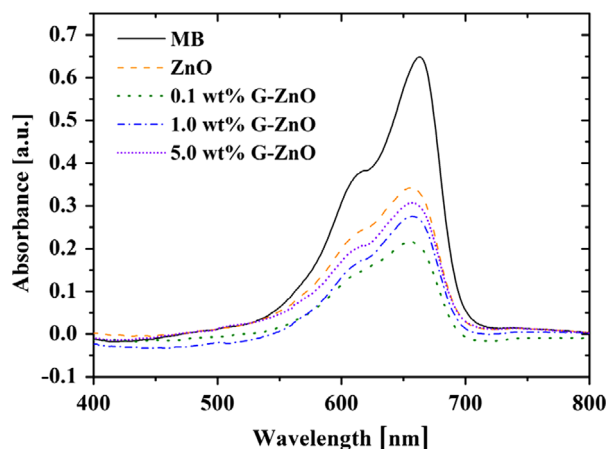


Fig. 8. Effect of graphene concentration on MB degradation after 2 h of UV illumination.

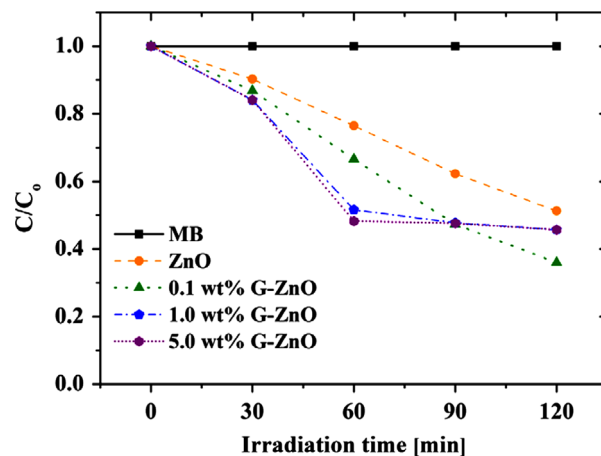


Fig. 9. Photocatalytic degradation of MB as a function of time by different graphene concentration films annealed at 300 °C temperature.

Table 1

Degradation efficiency of ZnO and G–ZnO thin films annealed at 300 °C.

Sample	ZnO	0.1 wt% G–ZnO	1.0 wt% G–ZnO	5.0 wt% G–ZnO
Degradation efficiency [%]	48.7	64.0	54.3	54.3

in Fig. 9. For  $t_{UV} < 1$  h, 1 and 5 wt% G–ZnO films showed better photocatalytic activity than that of 0.1 wt% because of the synergistic effect of graphene and ZnO, as shown in Fig. 9. However, for  $t_{UV} > 1$  h, the photocatalytic activity of 1 and 5 wt% films reduced, as compared to the activity of the 0.1 wt% film. As previously explained in the Experimental section, the film with 5 wt% graphene doping showed poor adhesion between ZnO and graphene sheets. This poor adhesion at higher graphene concentrations at longer time ( $t_{UV} > 1$  h) might produce graphene detachment from ZnO, which in turn hinders the synergistic effect and the photocatalytic activity at longer time.

The degradation efficiencies,  $D$ , with increasing graphene concentration for films annealed at 300 °C are presented in Table 1. After 2 h of UV irradiation, the 0.1 wt% sample exhibited the highest degradation efficiency (68.6%). It is well known that the absorption of light, charge carrier separation, and charge transportation play crucial roles during photocatalysis. Thus, the enhanced photocatalytic performance of the 0.1 wt% G–ZnO film is due to these characteristics, namely the increased light absorption of graphene and reduced recombination of the photo-generated electrons and holes in ZnO. Upon further increasing the graphene concentration, the photodegradation efficiency deteriorated, as shown in Table 1. This reduction is caused by increased light filtering and fewer photo-induced charge carriers in the G–ZnO composite; excessive graphene content could also facilitate recombination rather than allowing effective electron transport, which would contribute to the reduction in activity [33]. Thus, the optimal photocatalytic activity of the G–ZnO composites was attained with 0.1 wt% graphene content.

Table 2

Comparison of G–ZnO thin films with previous photocatalysis works.

Author	Method	Organic pollutant	Light and intensity	Remarks
Lv et al. [4]	Microwave assisted reaction using zinc nitrate, reduced graphene oxide (RGO) and carbon nanotube (CNT)	MB	365 nm UV light	ZnO–RGO–CNT composite powder with 3.9 wt% CNT gives 96% degradation of MB solution after 260 min
Liu et al. [22]	Microwave assisted non-aqueous method using ZnO and RGO	MB and Rhodamine B (RhB)	Visible light	RGO/ZnO powder with 0.0069 M Zn <sup>+</sup> concentration degrades RhB in 40 min and MB in 20 min under visible light
Liu et al. [33]	UV assisted photocatalytic reduction of graphene oxide by ZnO nanoparticles	Cr(IV)	365 nm UV light	RGO–ZnO composite powder with 1 wt% RGO removes 96% of Cr(IV) in 60 min
Present work	ESD coated G–ZnO thin films	MB	254 nm UV light	0.1 wt% G–ZnO composite thin film degrades 68% of MB in 120 min

Table 2 displays the results of photocatalytic experiments using the G–ZnO composite powder that were performed by various researchers. However, as previously mentioned, comparing the powder form of the photocatalyst to the thin film form is more significant. Thus, in our experiment, 68.6% MB degradation was observed after 2 h of UV irradiation for 0.1 wt% of G–ZnO thin films deposited by ESD. Hence, this ESD method can be used for the deposition of G–ZnO thin films for photocatalytic applications.

#### 4. Conclusions

G–ZnO composite thin films were successfully deposited using the ESD technique with a dispersion of graphene in a zinc acetate solution. Our experimental studies indicated that the incorporation of graphene enhances the photocatalytic performance: the 0.1 wt% G–ZnO film had the highest photo-degradation efficiency of MB of 68.6% after 2 h of UV irradiation. Increased light absorption and reduced charge recombination upon the introduction of graphene are responsible for the enhanced photocatalytic activity of the G–ZnO composite films.

#### Acknowledgments

This research was supported by the Converging Research Center Program through the Ministry of Education, Science and Technology (2013K000186) and B551179-08-03-00. This work was also supported by the Center for Inorganic Photovoltaic Materials (No. 2012-0001169) grant funded by the Korea government (MSIP).

#### References

- [1] H. Wang, S. Dong, Y. Chang, X. Zhou, X. Hu, Microstructures and photocatalytic properties of porous ZnO films synthesized by chemical bath deposition method, *Applied Surface Science* 258 (10) (2012) 4288–4293.
- [2] N. Padmavathy, R. Vijayaraghavan, Enhanced bioactivity of ZnO nanoparticles—an antimicrobial study, *Science and Technology of Advanced Materials* 9 (3) (2008) 035004.
- [3] J. Lv, W. Gong, K. Huang, J. Zhu, F. Meng, X. Song, Z. Sun, Effect of annealing temperature on photocatalytic activity of ZnO thin films prepared by sol–gel method, *Superlattices and Microstructures* 50 (2) (2011) 98–106.
- [4] T. Lv, L. Pan, X. Liu, Z. Sun, Enhanced photocatalytic degradation of methylene blue by ZnO–reduced graphene oxide–carbon nanotube composites synthesized via microwave-assisted reaction, *Catalysis Science and Technology* 2 (11) (2012) 2297.
- [5] B. Li, H. Cao, ZnO@graphene composite with enhanced performance for the removal of dye from water, *Journal of Materials Chemistry* 21 (10) (2011) 3346.
- [6] T. Xu, L. Zhang, H. Cheng, Y. Zhu, Significantly enhanced photocatalytic performance of ZnO via graphene hybridization and the mechanism study, *Applied Catalysis B: Environmental* 101 (3–4) (2011) 382–387.
- [7] K. Gopalakrishnan, H.M. Joshi, P. Kumar, L.S. Panchakarla, C.N.R. Rao, Selectivity in the photocatalytic properties of the composites of TiO<sub>2</sub> nanoparticles with B- and N-doped graphenes, *Chemical Physics Letters* 511 (4–6) (2011) 304–308.
- [8] R. Das, S. Ray, Zinc oxide—a transparent, conducting IR-reflector prepared by rf-magnetron sputtering, *Journal of Physics D: Applied Physics* 36 (2) (2003) 152.
- [9] A. Khoury, R. al Asmar, M. Abdallah, G.E.H. Moussa, A. Foucaran, Comparative study between zinc oxide elaborated by spray pyrolysis, electron beam evaporation and rf magnetron techniques, *Physica Status Solidi (a)* 207 (8) (2010) 1900–1904.
- [10] A. Hongsingthong, I. Afdi Yunaz, S. Miyajima, M. Konagai, Preparation of ZnO thin films using MOCVD technique with D<sub>2</sub>O/H<sub>2</sub>O gas mixture for use as TCO in silicon-based thin film solar cells, *Solar Energy Materials and Solar Cells* 95 (1) (2011) 171–174.
- [11] L. Lansiaert, E. Millon, J. Perrière, J. Mathias, A. Petit, W. Seiler, C. Boulmer-Leborgne, Structural properties of ZnO films grown by picosecond pulsed-laser deposition, *Applied Surface Science* 258 (23) (2012) 9112–9115.
- [12] Y. Sun, J.H. Seo, C.J. Takacs, J. Seifert, A.J. Heeger, Inverted polymer solar cells integrated with a low-temperature-annealed sol–gel-derived ZnO Film as an electron transport layer, *Advanced Materials* 23 (14) (2011) 1679–1683.
- [13] L. Hadjeris, L. Herissi, M.B. Assouar, T. Easwarakhanthan, J. Bougdira, N. Attaf, M.S. Aida, Transparent and conducting ZnO films grown by spray pyrolysis, *Semiconductor Science and Technology* 24 (3) (2009) 035006.
- [14] A. Hosseinmardi, N. Shojaei, M. Keyanpour-Rad, T. Ebadzadeh, A study on the photoluminescence properties of electrospray deposited amorphous and crystalline nanostructured ZnO thin films, *Ceramics International* 38 (3) (2012) 1975–1980.
- [15] K.S. Kim, Y. Zhao, H. Jang, S.Y. Lee, J.M. Kim, K.S. Kim, J.H. Ahn, P. Kim, J.Y. Choi, B.H. Hong, Large-scale pattern growth of graphene films for stretchable transparent electrodes, *Nature* 457 (7230) (2009) 706–710.
- [16] E. Kymakis, E. Stratakis, M.M. Stylianakis, E. Koudoumas, C. Fotakis, Spin coated graphene films as the transparent electrode in organic photovoltaic devices, *Thin Solid Films* 520 (4) (2011) 1238–1241.

- [17] M. Beidaghi, Z. Wang, L. Gu, C. Wang, Electrostatic spray deposition of graphene nanoplatelets for high-power thin-film supercapacitor electrodes, *Journal of Solid State Electrochemistry* 16 (10) (2012) 3341–3348.
- [18] V.H. Pham, T.V. Cuong, S.H. Hur, E.W. Shin, J.S. Kim, J.S. Chung, E.J. Kim, Fast and simple fabrication of a large transparent chemically-converted graphene film by spray-coating, *Carbon* 48 (7) (2010) 1945–1951.
- [19] H. Yoon, J.H. Woo, Y.M. Ra, S.S. Yoon, H.Y. Kim, S. Ahn, J.H. Yun, J. Gwak, K. Yoon, S.C. James, Electrostatic spray deposition of copper-indium thin films, *Aerosol Science and Technology* 45 (12) (2011) 1448–1455.
- [20] B.N. Joshi, H. Yoon, H.Y. Kim, J.H. Oh, T.Y. Seong, S.C. James, S.S. Yoon, Effect of zinc acetate concentration on structural, optical and electrical properties of ZnO thin films deposited by electrostatic spray on an ITO substrate, *Journal of the Electrochemical Society* 159 (8) (2012) H716–H721.
- [21] S.-M. Lam, J.-C. Sin, A.Z. Abdullah, A.R. Mohamed, Degradation of wastewaters containing organic dyes photocatalysed by zinc oxide: a review, *Desalination and Water Treatment* 41 (1–3) (2012) 131–169.
- [22] Y. Liu, Y. Hu, M. Zhou, H. Qian, X. Hu, Microwave-assisted non-aqueous route to deposit well-dispersed ZnO nanocrystals on reduced graphene oxide sheets with improved photoactivity for the decolorization of dyes under visible light, *Applied Catalysis B: Environmental* 125 (21) (2012) 425–431.
- [23] R.B. Draper, M.A. Fox, Titanium dioxide photosensitized reactions studied by diffuse reflectance flash photolysis in aqueous suspensions of TiO<sub>2</sub> powder, *Langmuir* 6 (8) (1990) 1396–1402.
- [24] C.S. Turchi, D.F. Ollis, Mixed reactant photocatalysis: intermediates and mutual rate inhibition, *Journal of Catalysis* 119 (2) (1989) 483–496.
- [25] K. Fuwa, B. Valle, The physical basis of analytical atomic absorption spectrometry. The pertinence of the Beer–Lambert law, *Analytical Chemistry* 35 (8) (1963) 942–946.
- [26] C. Yogi, K. Kojima, N. Wada, H. Tokumoto, T. Takai, T. Mizoguchi, H. Tamiaki, Photocatalytic degradation of methylene blue by TiO<sub>2</sub> film and Au particles–TiO<sub>2</sub> composite film, *Thin Solid Films* 516 (17) (2008) 5881–5884.
- [27] T. Lu, Y. Zhang, H. Li, L. Pan, Y. Li, Z. Sun, Electrochemical behaviors of graphene–ZnO and graphene–SnO<sub>2</sub> composite films for supercapacitors, *Electrochimica Acta* 55 (13) (2010) 4170–4173.
- [28] G. Wang, J. Yang, J. Park, X. Gou, B. Wang, H. Liu, J. Yao, Facile synthesis and characterization of graphene nanosheets, *Journal of Physical Chemistry C* 112 (22) (2008) 8192–8195.
- [29] Q. Xi, X. Chen, D.G. Evans, W. Yang, Gold nanoparticle-embedded porous graphene thin films fabricated via layer-by-layer self-assembly and subsequent thermal annealing for electrochemical sensing, *Langmuir* 28 (25) (2012) 9885–9892.
- [30] A.R. Marlinda, N.M. Huang, M.R. Muhamad, M.N. An'amt, B.Y. S. Chang, N. Yusoff, I. Harrison, H.N. Lim, C.H. Chia, S.V. Kumar, Highly efficient preparation of ZnO nanorods decorated reduced graphene oxide nanocomposites, *Materials Letters* 80 (2012) 9–12.
- [31] Y. Zhang, Z.-R. Tang, X. Fu, Y.-J. Xu, TiO<sub>2</sub>–Graphene nanocomposites for gas-phase photocatalytic degradation of volatile aromatic pollutant: is TiO<sub>2</sub>–graphene truly different from other TiO<sub>2</sub>–carbon composite materials?, *ACS Nano* 4 (12) (2010) 7303–7314.
- [32] P. Jongnavakit, P. Amornpitoksuk, S. Suwanboon, N. Ndiege, Preparation and photocatalytic activity of Cu-doped ZnO thin films prepared by the sol–gel method, *Applied Surface Science* 258 (20) (2012) 8192–8198.
- [33] X. Liu, L. Pan, Q. Zhao, T. Lv, G. Zhu, T. Chen, T. Lu, Z. Sun, C. Sun, UV-assisted photocatalytic synthesis of ZnO–reduced graphene oxide composites with enhanced photocatalytic activity in reduction of Cr(VI), *Chemical Engineering Journal* 183 (2012) 238–243.